Aerospace Science and Technology 120 (2022) 107251

Contents lists available at ScienceDirect

Aerospace Science and Technology

www.elsevier.com/locate/aescte

Stochastic optimization of high-altitude airship envelopes based on kriging method

Adrián García-Gutiérrez *, Jesús Gonzalo, Diego Domínguez, Deibi López

Universidad de León, Aerospace Engineering Area, Campus de Vegazana S/n, León, 24071, Spain

ARTICLE INFO

Article history:
Received 30 June 2021
Received in revised form 25 November 2021
Accepted 25 November 2021
Available online 30 November 2021
Communicated by Jérôme Morio

Keywords:
Airship
Drag reduction
Robust design
Stochastic optimization

ABSTRACT

High-altitude airships can be used to transport substantial payloads to the stratosphere and remain there over long periods of time. In this paper, an algorithm for the design of high-altitude airship envelopes, accounting for uncertainties, is developed and applied. The algorithm is based on the non-intrusive polynomial chaos expansion scheme, which is employed to build a stochastic kriging metamodel. Two uncertainties are examined and characterized: 1) the stratospheric wind fluctuations using reanalysis datasets and 2) the variability in the turbulence levels. The method results are discussed to address the relevancy of the uncertainties. It is found that the drag coefficient of stratospheric envelopes can vary by as much as 30 percent. As a case of study, an ideal stratospheric airship is considered, operating at an altitude of 20 km, at a latitude of 30^{c}N and carrying a payload of 250 kg. The baseline design follows the shape of the ZHIYUAN-1 envelope and the cost function to be minimized is the average mission drag coefficient. Due to the new method, a significant reduction (4%) of the average drag of the aircraft is achieved.

1. Introduction

In recent years, there is a growing interest in High Altitude Pseudo-Satellites (HAPS) due to their relevant applications in Telecommunications, Earth Observations and Defense [1]. Although the technical difficulties are still very defiant, recent advances in the field of solar cells, batteries or fabric materials have overcome traditional limitations and notably improved the feasibility of those platforms.

Energy management onboard the platform is a key issue that limits platform size and flight endurance. Related to this, the drag coefficient of the airship plays a very relevant role, as most of the energy consumption required to keep the platform flying is used to compensate aerodynamic drag. At the end, that means drag value strongly conditions the required size of the batteries, the solar panels and even the propellers [2]. About the 60-70% of the total drag is due to the hull [3]. Thus, to reduce the total drag, the first step is to improve the aerodynamic design of the hull.

Previous studies have explored the shape optimization of stratospheric airship [3,4] and, also, have studied their aerodynamic characteristics [5][6][7] and the effect of the propeller [4].

However, these studies suffer from the fact that they do not address the robustness of the designs. Therefore, a poor performance might be obtained under off-design operational conditions attending to mission phases, maneuvers or environmental conditions.

Typically, the robustness of designs has been analyzed in multidisciplinary studies [8,9] integrating different disciplines such as energy management, thermal control, structural and aerodynamic design [10,11].

This study, however, focuses on the way in which the robust aerodynamic design of stratospheric airship hulls can improve the overall performance of the mission. Although a full discussion of all the uncertainties in the hull design is beyond the scope of this study, two of the most relevant environmental effects impacting aerodynamics are considered: the variation of the wind intensity and air turbulence levels.

Despite many designers consider constant wind (for a fixed altitude) in their analysis, the wind intensity is better fit by a Weibull distribution [12]. The impact of this variation in the mean drag coefficient of the hull has received scant attention in the research literature. Furthermore, due to the low density, the Reynolds number of these airships is lower than in the traditional ones. Thus, aerodynamic coefficients can be significantly affected by wind turbulence levels in the far-field region [13].

Generally speaking, the introduction of uncertainties into the design has been done following different approaches. For exam-

* Corresponding author.
E-mail address: agarcg@unileon.es (A. García-Gutiérrez).

https://doi.org/10.1016/j.ast.2021.107251
1270-9638/

Nomenclature

Au_i	Parameters of the CST parameterization
$C_{D,v}$	Volumetric drag coefficient
$C_{D,p}$	Volumetric pressure drag coefficient
$C_{D,v}$	Volumetric friction drag coefficient
$\mathcal{C}_D$	Stochastic operator used to compute the $C_{D,v}$
$\hat{\mathcal{C}}_D$	Approximation of the function $\mathcal{C}_D$
$C_{N_2}^{N_1}$	Class function
CFD	Computational fluid dynamics
CDF	Cumulative distribution function
E	Expectation operator
F	Cost function
FFD	Free-form deformation
HAPS	High-Altitude Pseudo-Satellites
k	Turbulence kinetic energy
K_v	Speed constant
L	Airship length
Ma	Mach number
MC	Monte Carlo method
MSE	Mean squared error
NIPC	Non-intrusive polynomial chaos
PDF	Probability density function
RBF	Radial basis function
Re	Reynolds number
RMS	Root mean square
$\mathbf{X}$	Multivariate random variable
S_i	Univariate random variable/ Component shape function
SL	Sea level
Su	Shape function equation for the upper surface
Tu_∞	Turbulence levels (%)
U	Wind velocity
UQ	Uncertainty Quantification
V	Airship volume
$\mathbf{Y}$	Multivariate stochastic function
$\hat{\mathbf{Y}}_i$	NIPC expansion coefficients
$\overline{w}$	Velocity
α	Angle of attack
$\Delta\zeta_{hull}$	Thickness of the trailing edge
ϕ	One dimensional polynomial basis function
Φ_i	Multivariate orthogonal polynomial basis function
ψ	Dimensionless coordinate x/c
ζ	Dimensionless coordinate y/c
μ	Kinematic viscosity/mean
ρ	Air density
ν	Kinematic viscosity
ν_t	Turbulence viscosity
ω	Turbulence specific dissipation rate
σ	Standard deviation

ple, Kumar [14] combined the non-intrusive polynomial chaos (NIPC) with adjoint formulations using the CFD code SU2 [15]. The method was applied to a 2D transonic airfoil under uncertainties in the Mach number and angle of attack. However, these uncertainties were not related to real operational conditions. The study was focused on the design method and, thus, the uncertainty modeling was not studied in depth. The main disadvantage of this method is that the adjoint formulation can be difficult to implement in some cases —the adjoint system equations are not the same as the equations of the system that is being modeled, so the solvers have to be customized—.

As alternative, Liatsikouras et al. [16] proposed a new method based on evolutionary algorithms combined with the non-intrusive Polynomial Chaos. They applied it to the optimization of 2D airfoils and S-Bend Duct. This method can be easily adapted to a broad range of situations, however, it is based on an on–line trained metamodel implemented within an evolutionary algorithm. This might be a problem if the computational load is high enough to require High Performance Computing centers. In that case, an off-line approach is more adequate.

Within the naval field, Serani et al. [17] proposed a new algorithm for ship hull optimization based on 4 steps 1) dimensionality reduction of the design space, 2) adaptive metamodeling, 3) uncertainty quantification and 4) multi-objective global optimization algorithms. Its final design achieved an expected mean value of total drag of -2.8%.

Following previous studies on robust optimization, the design algorithm consists of three main parts:

1. First, we determine the performance of a particular design taking into account the different uncertainties following one of the available Uncertainty Quantification (UQ) techniques. The NIPC seems to be the best option based on its fast convergence and its easy implementation.
2. Second, a metamodel is built using results from CFD simulations. That metamodel will be used to easily compute the mean drag coefficient of the airship as a function of some design variables. There are several kinds of metamodels (also known as surrogate models), but kriging metamodels provide a good balance between computational resources and accuracy [18][19]. Although RBF (Radial basis function) networks have not been used in this work, they can be a good alternative, as shown in several studies [20].
3. Finally, a non linear optimization solver is used to compute the optimal design, running sequentially the metamodel looking for minima.

The remaining part of the paper proceeds as follows: Section 2 examines the non-intrusive Polynomial Chaos and how it can be used for the robust design of airships. Next, Section 3 describes how to build the metamodel based on the kriging theory and which is the best parameterization of the geometry. Then, the physics, solver and mesh setup of the CFD simulations are described together with their validation in Section 4. The overall view of the design methodology is finally given in Section 5, so it can be applied to a realistic case of study in Section 6. At last, the relevant conclusion is detailed in Section 7.

2. Uncertainty quantification using non-intrusive polynomial chaos

As it has been mentioned previously, the NIPC has been selected as the method of uncertainty quantification. There are other methods than can be used as alternative, such as Monte Carlo simulations [21] or most probable point based methods [22]. Many of these methods have proven to have fast convergence and simple implementation such as those studied by Piazzola et al. [23] and Quagliarella et al. [24]. Among those, the NIPC methods have been used for this work. Alternative methods could be implemented in a similar way.

Previous research has established how NIPC can be used to determine the uncertainty effects in the aerodynamic coefficients [25,26]. The reader can refer to [27] and the references therein for the mathematical development of the theory. Details of how the

general theory can be applied to the particular case of the hull aerodynamics can be found below.

In this case, the stochastic function to approximate is the volumetric drag coefficient of the hull $C_{D,v}$, which is a stochastic function because it depends on (at least) two stochastic variables: the wind intensity (U) and the turbulent levels Tu_∞. The NIPC method approximates the stochastic solution $C_{D,v}(U, Tu_\infty)$ of our design problem by a finite linear combination of orthogonal polynomials Φ_i of the 2 independent random variable $\mathbf{S} = (U, Tu_\infty) = (S_1, S_2) \in \mathbb{R}^2$. So, the Pth order approximation can be written as:

$$\mathbf{C_{D,v}}(\mathbf{S}) \approx \hat{\mathbf{C}}_{\mathbf{D,v}}(\mathbf{S}) := \sum_{i=0}^{M} \hat{\mathbf{C}}_{\mathbf{D,v,i}} \Phi_i(\mathbf{S}), \tag{1}$$

where $\hat{\mathbf{C}}_{\mathbf{D,v,i}}$ are the NIPC expansion coefficients, and $\Phi_i(\mathbf{S})$ are the multivariate orthogonal polynomial basis function which can be written in terms of one-dimensional polynomial basis function $\phi_i^{(l_i)}(S_i)$ of each random variable (U or Tu_∞) according to the following relation:

$$\Phi_i(\mathbf{S}) = \prod_{i=1}^{N} \phi_i^{(l_i)}(S_i), \tag{2}$$

where $\sum l_i \leq P$ and the coefficient M is the total number of basis functions and can be calculated as $M = \binom{N+P}{M}$.

The polynomial base is orthogonal under the following vector product:

$$\langle \phi_i(S_i), \phi_j(S_i) \rangle = \delta_{ij} \langle \phi_i(S_i)^2 \rangle, \tag{3}$$

where $< \cdot, \cdot >$ is defined as the expectation operator:

$$\langle f(S_i), g(S_i) \rangle = \int f(S_i) g(S_i) \rho_i(S_i) \mathrm{d}S_i, \tag{4}$$

being $\rho_i(S_i)$ the probability density function corresponding to the ith random variable S_i and δ_{ij} the Kronecker delta function.

In order to compute each of the coefficients $\hat{\mathbf{C}}_{\mathbf{D,v,i}}$, we can apply the expectation operator to the orthogonal polynomial $\Phi_i(\mathbf{S})$ which yields to the following equation:

$$\hat{\mathbf{C}}_{\mathbf{D,v,i}} = \frac{1}{\langle \phi_i(\mathbf{S})^2 \rangle} \int \mathbf{C_{D,v}}(\mathbf{S}) \Phi_i(\mathbf{S}) \varrho(\mathbf{S}) \mathrm{d}\mathbf{S}, \tag{5}$$

where ϱ is the joint probability density function $\varrho(\mathbf{S}) = \prod \rho_i(S_i)$.

The integral of Eq. (5) can be approximated by quadrature, so the following expression is obtained:

$$\hat{\mathbf{C}}_{\mathbf{D,v,i}}(U, Tu_\infty) = \sum_{k_1=1}^{m_1} \sum_{k_2=1}^{m_2} \mathbf{C_{D,v}}(U_{k_1}, Tu_{\infty_{k_2}}) \frac{\Phi_i(U_{k_1}, Tu_{\infty_{k_2}})}{\langle \Phi_i(U_{k_1}, Tu_{\infty_{k_2}})^2 \rangle} \prod_{j=1}^{q} \omega_j, \tag{6}$$

being U_{k_j} and $Tu_{\infty_{k_j}}$ with $j = 1 \cdots q$ the quadrature points of the j-component of the random vector $\mathbf{S}$, m_i denotes the integration points number of each random variable and ω_j is the quadrature jth-dimension weight of the point $\mathbf{S_{k_j}}$.

Once the coefficients have been computed, the expected value μ and variance σ of $\mathbf{Y}(\mathbf{S})$ can be estimated using the following equations:

$$\mu(\mathbf{C_{D,v}}) \approx \hat{\mathbf{C}}_{\mathbf{D,v,0}}, \tag{7}$$

$$\sigma(\mathbf{C_{D,v}}) \approx \sqrt{\sum_{i=1}^{p} \langle \phi_i^2 \rangle \hat{\mathbf{C}}_{\mathbf{D,v,i}}}. \tag{8}$$

Thus, to determine the mean and standard deviation of a particular hull design, it is only needed to evaluate that design in each of the quadrature points previously defined.

3. Parameterization and kriging metamodeling

Although the NIPC theory reduces the number of CFD simulations needed to determine the mean $C_{D,v}$ of each design, the time that takes to evaluate all the quadrature points remains too high. Thus, it is still necessary to create a metamodel in order to find the optimal design. That metamodel will compute the estimated mean drag coefficient for certain design variables. The number of these design variables should be as low as possible although the parameterization has to be able to represent the geometry of the hull correctly. That is why it is important to correctly choose the shape parameterization. Up to this point, there are many families of parameters which can be used to do that. For example, Du & Leifur [28] chose B-splines while Mader & Martins [29] used Free-form deformation (FFD) instead. However, the CST (Class/Shape Transformation) Universal parametric geometry representation method [30] was chosen in this case. The main reason is that this method has been shown to accurately represent any realistic hull geometry with a minimum number of variables [31]. It is worth noting that, in this method, the number of variables to be used can be chosen by the user, depending on the required accuracy. This differs from other methods such as the Gertler-58 series, in which the number of variables is always 5.

A brief description of how to apply it is given below.

First, the non-dimensional spatial coordinates are defined as $\psi = x/c$ and $\zeta = y/c$. Then, the so-called component shape functions are defined as:

$$S_i(\psi) = K_i \psi^i (1-\psi)^{n-1}, \tag{9}$$

in which K_i is computed with the following formula:

$$K_i = \binom{n}{i} = \frac{n!}{i!(n-i)!}, \tag{10}$$

so the overall shape function equation for the upper surface is:

$$Su(\psi) = \sum_{i=1}^{n} Au_i \cdot S_i(\psi). \tag{11}$$

On the other hand, the class function is defined as:

$$C_{N_2}^{N_1}(\psi) = \psi^{N_1} (1-\psi)^{N_2}, \tag{12}$$

and, depending on the thickness of the trailing edge:

$$\Delta\zeta_{hull} = \frac{y_{TE}}{c}, \tag{13}$$

the hull generatrix is given by the following expression:

$$\zeta_{hull} = C_{N_2}^{N_1}(\psi) \cdot Su(\psi) + \psi \cdot \Delta\xi_{hull}, \tag{14}$$

in which the coefficients Au_i for a particular design can be determined using least squares method.

Once the geometry parameterization is done, the metamodel creation can be started. Kriging techniques interpolate the value of a random field (the mean $C_{D,v}$ in our case) at an unknown design parameters from previously compute designs. Kriging computes the best linear unbiased estimator (refer from now on as $\hat{C}_D(x_0)$) based on a stochastic model determined by the expectation and covariance function of the random field [32].

Thus, the kriging metamodel is given by a linear combination [33]:

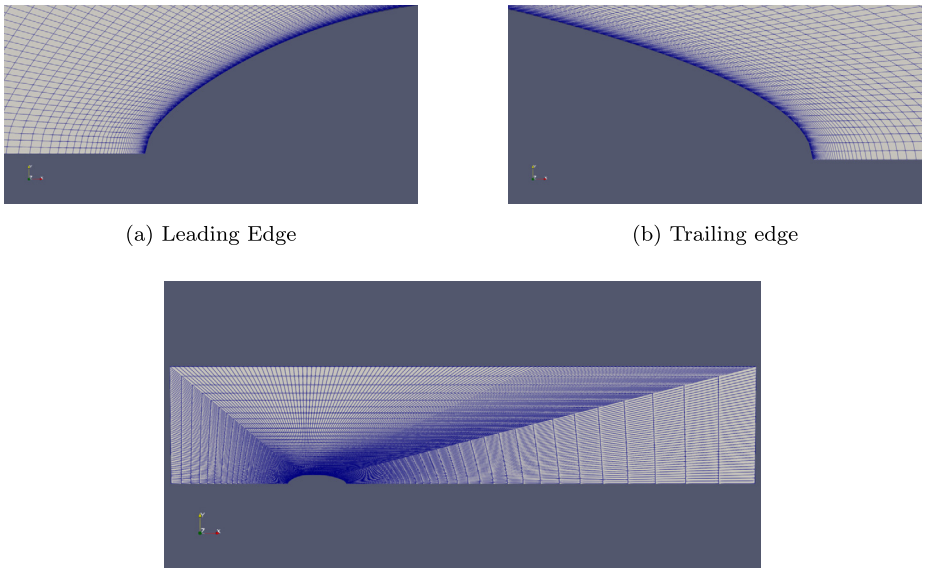

(a) Leading Edge (b) Trailing edge

Figure 1: overview of the mesh

Fig. 1. Overview of the mesh.

$$\hat{C}_D(x_0) = \sum_{i=1}^{n} w_i(x_0) C_D(x_i), \tag{15}$$

in which the parameters w_i are computed so the variance:

$$\sigma_k^2(x_0) := \mathrm{Var}\left(\hat{C}_D(x_0) - C_D(x_0)\right), \tag{16}$$

is minimized subject to the unbiasedness condition:

$$\mathrm{E}[\hat{Z}(x) - Z(x)] = \sum_{i=1}^{n} w_i(x_0)\mu(x_i) - \mu(x_0) = 0. \tag{17}$$

In general, at first, coarse kriging metamodel is generated. Some of the samples are reserved as test points, so the Mean Square Error MSE can be computed as:

$$MSE = \frac{1}{n}\sum_{1}^{n}(\hat{C}_D(x_i) - C_D(x_i))^2. \tag{18}$$

Then, that error is reduced adding infill points to the model [34, 35].

In the present study, the Kriging metamodel has been implemented using the pyKriging [36] toolbox, recently used in other aerodynamic studies such as Chen et al. [37] and Habermann et al. [38].

4. CFD model and validations

As it has been mentioned before, a large number of CFD simulations are required to build the stochastic metamodel. To minimize the computational time, only axisymmetric simulations are considered, which have obtained good results in previous studies [39] about airship aerodynamics. Steady RANS equations are solved by the SIMPLE algorithm with a second order upwind scheme applied to the convection terms. For all the simulations no wall function has been used and the maximum size of the first cell was selected so y^+ is equal or less than 1. OpenFoam has been selected as the CFD solver due to: 1) it has been largely proven for external aerodynamics [40], and 2) its automatic parallelization capabilities. This election is consistent with past studies. For example, Jouebert and Le Roy [41] studied, using OpenFoam, the effect of the grid coarseness and numerical schemes on Lighter-than-Air (LTA) aircraft.

For each simulation, a rectangular domain and a structured, hexagonal, 2-dimensional mesh around each design was created using the meshing tool blockMesh, supplied in OpenFoam [42]. Each mesh file has 2.4×10^4 cells and the domain dimensions are $[-2.5L,\ 7.5L] \times [-2.5L,\ 2.5L]$ being the airship (of length L) centered at the point (0, 0). An overview of the mesh used can be seen in Fig. 1.

Based on previous work [43][44][5], the RANS model selected is the SST Menter $k-\omega$ [45] although other models such as realizable $K-\epsilon$ and Spalart-Allmaras are frequently used [46]. In this model, the equations to solved are:

$$\frac{\partial \bar{u}_i}{\partial x_i} = 0, \tag{19}$$

$$\frac{\partial \bar{u}_i}{\partial t} + \bar{u}_j\frac{\partial \bar{u}_i}{\partial x_j} + \overline{u'_j\frac{\partial u'_i}{\partial x_j}} = \bar{f}_i - \frac{1}{\rho}\frac{\partial \bar{p}}{\partial x_i} + \nu\frac{\partial^2 \bar{u}_i}{\partial x_j \partial x_j}. \tag{20}$$

The eddy viscosity can be computed as $\nu_T = \frac{k}{\omega}$, while k and ω are calculated resolving the following PDEs:

$$\frac{\partial(\rho k)}{\partial t} + \frac{\partial(\rho u_j k)}{\partial x_j} = P - \beta^*\rho\omega k + \frac{\partial}{\partial x_j}\left[(\mu + \sigma_k\mu_t)\frac{\partial k}{\partial x_j}\right], \tag{21}$$

$$\frac{\partial(\rho\omega)}{\partial t} + \frac{\partial(\rho u_j \omega)}{\partial x_j} = \frac{\gamma}{\nu_t}P - \beta\rho\omega^2 + \frac{\partial}{\partial x_j}\left[(\mu + \sigma_\omega\mu_t)\frac{\partial \omega}{\partial x_j}\right] + 2(1-F_1)\frac{\rho\sigma_{\omega 2}}{\omega}\frac{\partial k}{\partial x_j}\frac{\partial \omega}{\partial x_j}, \tag{22}$$

in which the following closure coefficients and auxiliary relations are used:

$$P = \tau_{ij}\frac{\partial u_i}{\partial x_j}, \tag{23}$$

$$\tau_{ij} = \mu_t\left(2S_{ij} - \frac{2}{3}\frac{\partial u_k}{\partial x_k}\delta_{ij}\right) - \frac{2}{3}\rho k\delta_{ij}, \tag{24}$$

$$S_{ij} = \frac{1}{2}\left(\frac{\partial u_i}{\partial x_j} + \frac{\partial u_j}{\partial x_i}\right), \tag{25}$$

$$\mu_t = \frac{\rho a_1 k}{\max(a_1\omega, \Omega F_2)}, \tag{26}$$

$$F_1 = \tanh\left(\arg_1^4\right), \tag{27}$$

$$\arg_1 = \min\left[\max\left(\frac{\sqrt{k}}{\beta^*\omega d}, \frac{500\nu}{d^2\omega}\right), \frac{4\rho\sigma_{\omega 2}k}{\mathrm{CD}_{k\omega}d^2}\right], \tag{28}$$

$$\mathrm{CD}_{k\omega} = \max\left(2\rho\sigma_{\omega 2}\frac{1}{\omega}\frac{\partial k}{\partial x_j}\frac{\partial \omega}{\partial x_j}, 10^{-20}\right), \tag{29}$$

$$F_2 = \tanh\left(\arg_2^2\right), \tag{30}$$

$$\arg_2 = \max\left(2\frac{\sqrt{k}}{\beta^*\omega d}, \frac{500\nu}{d^2\omega}\right). \tag{31}$$

The turbulence free-stream boundary conditions [47] are related to the inflow velocity U and the turbulent levels Tu_∞ by the following equations:

$$k = \frac{3}{2}(UTu_\infty)^2, \tag{32}$$

$$\omega = \frac{\sqrt{k}}{l}, \tag{33}$$

in which l is the turbulent length scale, estimated as the 0.5% of the airship length.

In order to validate the mesh and CFD configuration, the results obtained for the ZHIYUAN-1 [48] are compared with those of Manideep and Rajkumar [39] and Wang, Fu, Duan and Shan [48]. The generatrix is given by the following equations:

$$y = \begin{cases} f_r'[r_n F_1(z) + k_1 F_2(z) + G_1(z)]^{1/2} & 0 < x < x_m, \\ & z = \frac{x}{x_m}, \\ f_r'[s_t^2 F_3(z) + \left(\frac{1-x_m}{x_m}\right)^2 k_1 F_4(z) + G_2(z)]^{1/2} & x_m < x < x_p, \\ & z = \frac{1-x}{1-x_m}, \\ f_r'[c_p(1-z)] & x_p < x < 1, \\ & z = x, \end{cases} \tag{34}$$

in which:

$$F_1(z) = -2z(z-1)^3, \tag{35}$$

$$F_2(z) = -z^2(z-1)^2, \tag{36}$$

$$G_1(z) = z^2(3z^2 - 8z + 6), \tag{37}$$

$$F_3(z) = -z^2(z-1)^3, \tag{38}$$

$$F_4(z) = -z^3(z-1)^2, \tag{39}$$

$$G_2(z) = z^3(6z^2 - 15z + 10), \tag{40}$$

and the constants $x_m = 0.3935$, $x_p = 0.7570$, $r_n = 0.5071$, $k_1 = 0.2913$, $c_p = 2.7351$, $f_r' = 0.1516$ and $s_t = 3.2361$. The CST coefficients will be calculated in the Section 6.

The case of simulation corresponds to a Reynolds number $\mathrm{Re} = \frac{\rho v L}{\mu} = 2.4 \times 10^6$.

A grid verification study was conducted by varying the number of total cells. Five different meshes were tested, the results of which can be seen in Table 1. Mesh number 4 was chosen to reduce the calculation time while maintaining sufficient accuracy. In all cases, the y^+ number remains below 1.

Fig. 2 shows a good agreement between studies for the distribution of the pressure coefficient c_p. The $C_{Dv} = \frac{2D}{\rho V_\infty^2 S}$ obtained is 2.42×10^{-2} which differs only a 1.4% from the results of Wang, Fu, Duan & Shan [48] and 5.9% from Manideep & Rajkumar [39].

Table 1
Grid verification study.

Grid	C_{Dv}	% difference (finest grid)	N cells
1	2.19×10^{-2}	-9.7%	1.6×10^4
2	2.31×10^{-2}	-5.1%	1.8×10^4
3	2.4×10^{-2}	-1.2%	2.0×10^4
4	2.42×10^{-2}	-0.5%	2.4×10^4
5	2.43×10^{-2}	0	2.8×10^4

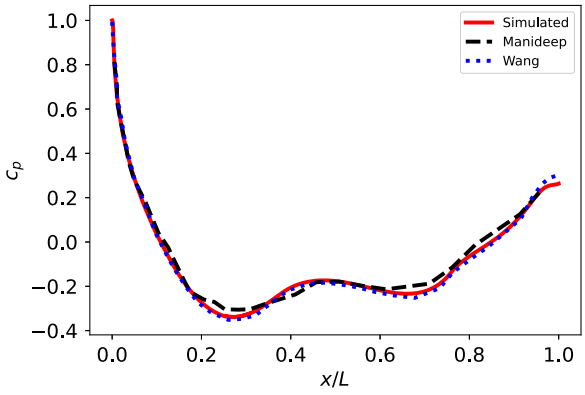

Fig. 2. Distribution of c_p along the airship length.

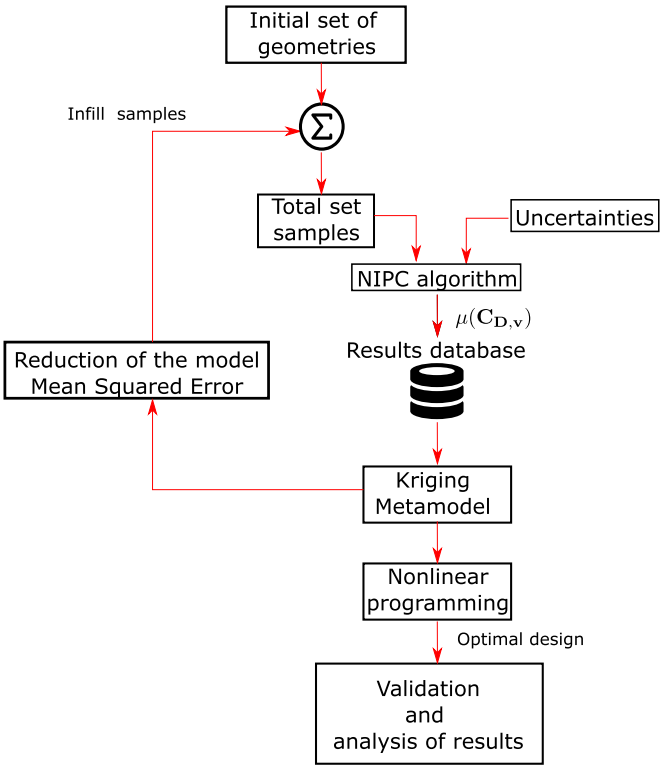

Fig. 3. Flow diagram of the proposed optimization algorithm.

5. Design methodology

Once the theory of the NIPC and the kriging techniques has been review, it is time to join both theories in order to solve the aerodynamic optimization problem. That can be resumed into the following steps:

1. The geometry of a baseline design is parameterized using a certain number of parameters. For each of that parameters,

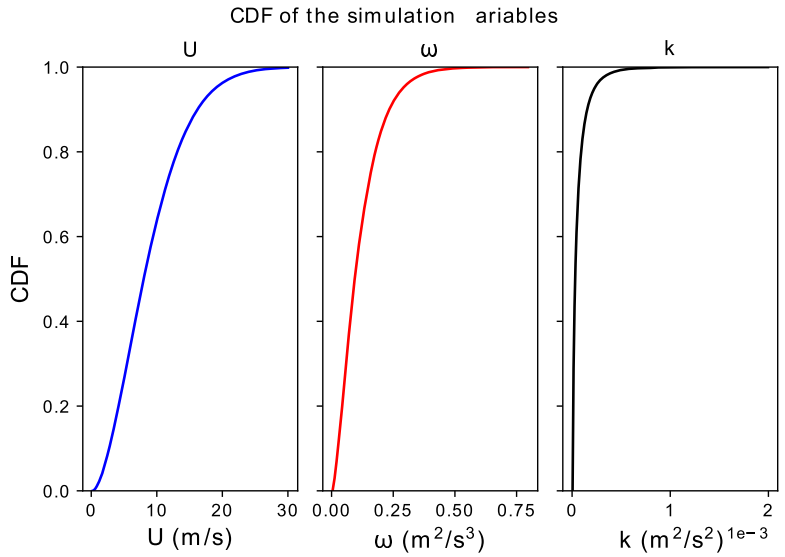

Fig. 4. Cumulative distribution function of wind intensity U, turbulent kinetic energy k and specific turbulent dissipation rate ω.

its interval of validity is determined. The number of variables should be set by the user according to the desired accuracy.
2. The design space, defined by the previous intervals, is randomly sampled, obtaining N different hull geometries to evaluate. This is usually done applying the Latin hypercube sampling technique [49].
3. Each of the geometries is evaluated, computing its mean $C_{D,v}$ using the NIPC.
4. Once the results are obtained, the first kriging metamodel is created. Some of the results are used as test points.
5. To reduce the Mean Squared Error of the model, new infill points are originated and evaluated.
6. The previous step is repeated until the MSE is sufficiently small.
7. Then, the metamodel is ready to be use by any nonlinear programming solver. The results of the optimization is the geometry which has the lower mean $C_{D,v}$.
8. Finally, the design can be validated using, for example, a Monte Carlo experiment. The results can be also analyzed to gain insights of the problem physics.

In Fig. 3, the flow diagram of the optimization algorithm is shown with all its relevant parts.

It is worth noting that, in this case, the kriging model has as input variables the geometrical parameters of the hull. The output of the model is the average drag coefficient, taking into account the probability distribution of the wind speed and turbulence index. The uncertainty associated with these two variables should not be confused with that of the kriging model. To train the metamodel, therefore, a database is required in which we have combinations of geometric parameters and the average resistance coefficients obtained with them. This coefficient is estimated for each combination of geometric variables using the UQ algorithm.

Due to the large number of simulations required by the optimization algorithm, an adequate parallelization method should be used. Taking advantage of the properties of the UQ algorithm, the following method based on supercomputing is proposed:

1. For each design, the CFD simulations of all the quadrature points are configured in a local workstation.
2. Then, the different cases are uploaded to the supercomputing center. Each of the cases can be run by a different computer node.
3. Likewise, each of the simulation is easily parallelized inside the node thanks to OpenFoam.
4. Finally, the results are recompile in the local workstation where the metamodel is built.

Thus, two levels of parallelization can be found. This makes the algorithm easily scalable to a higher number of uncertainties, design variables or CFD complexity.

6. Case of study

Next, we apply the optimization algorithm to a HAPS airship operating in the stratosphere (20 km) at a latitude of 30°N. That airship carries 250 kg of payload which means that its length would be around $L = 250$ m with today's technology [1].

6.1. UQ algorithm

Following the statistical study done in previous works [50], the cumulative distribution of the wind can be computed based on NCEP Reanalysis data provided by the NOAA/OAR/ESRL PSL, Boulder, Colorado, USA [51]. As it has been mentioned before, that wind intensity follows a Weibull distribution, so the probability density function (PDF) is given by the equation:

$$f(t) = \frac{\beta}{\eta}\left(\frac{t-\gamma}{\eta}\right)^{\beta-1} e^{-\left(\frac{t-\gamma}{\eta}\right)^{\beta}}, \tag{41}$$

in which η is the scale parameter, β is the shape parameter and γ is the location parameter. Following a least-squares adjustment, the parameter of the Weibull distribution which best fit the observational data are:

$$\eta = 9.715, \qquad \beta = 1.672, \qquad \gamma = 0.202. \tag{42}$$

Hence, the mean wind intensity is 8.9 m/s.

Then, it is needed to estimate the probabilistic distributions of the turbulence levels. However, the wind data at that height is scarce and a full study of the stratospheric characteristics is out of the scope of the present study. In this study, the approach followed in [26] is adopted: the turbulence levels will be assumed to follow a normal distribution of mean $Tu_{\infty} = 0.07\%$ and standard deviation $\sigma = 0.03\%$.

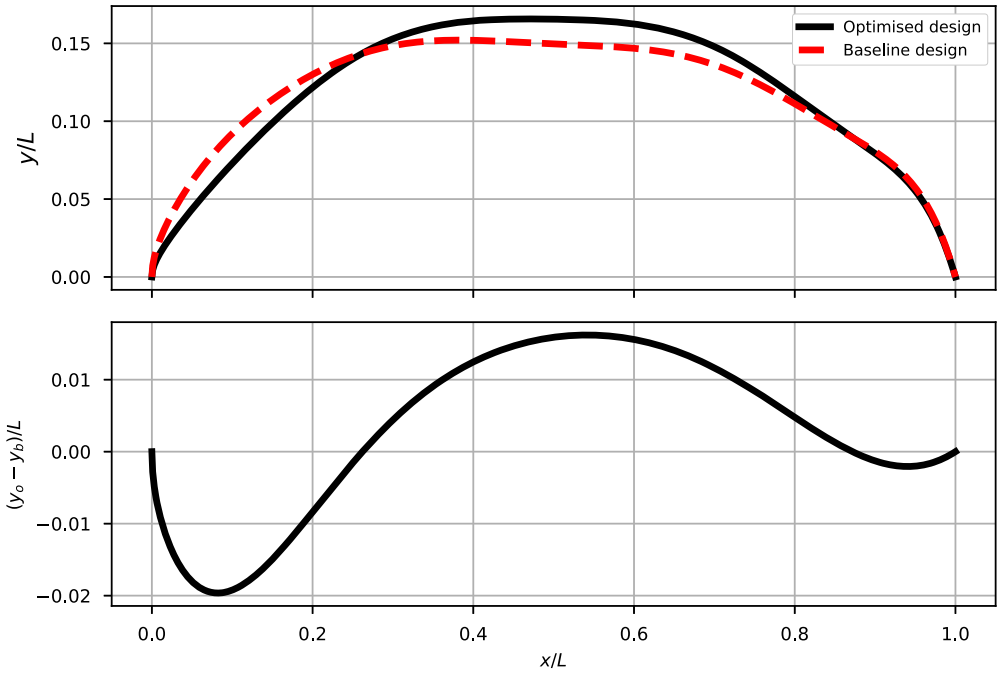

Fig. 5. Comparison of the geometries. Top image: optimal hull geometry compared against the baseline design. Bottom image: difference between the optimal design (y_o) and the baseline design (y_b).

The joint distribution of the wind intensity and turbulence levels affects the turbulent kinetic energy k and specific turbulent dissipation rate. Fig. 4 shows the different CDFs of the variables which affects the CFD simulations.

Once the probabilistic distribution of the wind intensity and turbulence levels is determined, the UQ method has to be configured. Both, the order of polynomial expansion and the one of quadrature, are set to 3 as a trade-off between accuracy and computational cost. Therefore, Equation (5) will be approximated by evaluating $\mathbf{C_{D,v}}(U_{k_1}, TL_{k_q})$ at 16 different quadrature points, according to Equation (6). In this way, the average resistance coefficient can be determined.

6.2. Metamodel generation

After the NIPC model is configured, it is time to build the kriging model. The first step is to discretize the hull geometry and determined in which range the parameters can vary. As baseline design, the ZHIYUAN-1 geometry was selected, given by Equation (34). If the airship length is set to $L = 250$ m, the volume is $V = 7.5 \times 10^5$ m^3. The optimization is done for a constant airship length (so the Reynolds number is equivalent for all the cases) and volume.

Then, the CST method is applied. The number of parameters (Au_i) for this method was fixed to 8 because it was enough to almost replicate the baseline geometry. These will be the design variables of this case of study. For the baseline design, this parameter were computed using the least squares methods obtaining:

$$\begin{aligned} Au_{0b} &= 0.0868, \quad Au_{1b} = 0.1863, \\ Au_{2b} &= 0.0354, \quad Au_{3b} = 0.4371, \\ Au_{4b} &= -0.3458, \quad Au_{5b} = 0.7976, \\ Au_{6b} &= -0.2756, \quad Au_{7b} = 0.7052. \end{aligned}$$

In order to find the optimal geometry, we found the metamodel $\hat{f}$ which compute the mean volumetric drag coefficient in function of that 8 design variables. To reduce the computational requirements, the design variables are constrained to the interval

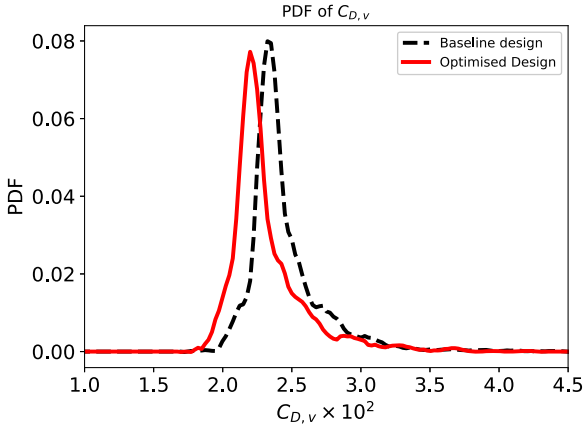

Fig. 6. PDF of the $C_{D,v}$ for both designs.

$Au_i \in Au_{ib} \pm 0.05$ although it is enough to represent all the reasonable designs. Firstly, 200 samples were randomly generated by means of the Latin hypercube sampling technique. These samples are evaluated, each one 14 times (one per quadrature point), and the results are introduced in the kriging metamodel. From these 200 points, 50 were selected as test points. Then, using the Mean Square Error MSE as the infill criteria [52] another 800 samples are generated and evaluated, of which 200 are test points. Thereafter, the MSE was small enough ($MSE < 10^{-3}$), so the third phase of the algorithm design can be started. In any case, the number of kriging points will vary depending on the required accuracy and the characteristics of the problem in question.

6.3. Non linear optimization and validation

Once the metamodel is finished, it is time to solve the nonlinear optimization problem. In order to do that, there are different algorithms such as the Nelder-Mead simplex algorithm or the Sequential Least Squares Programming. However, the optimal design can be very different from the baseline design, so it is bet-

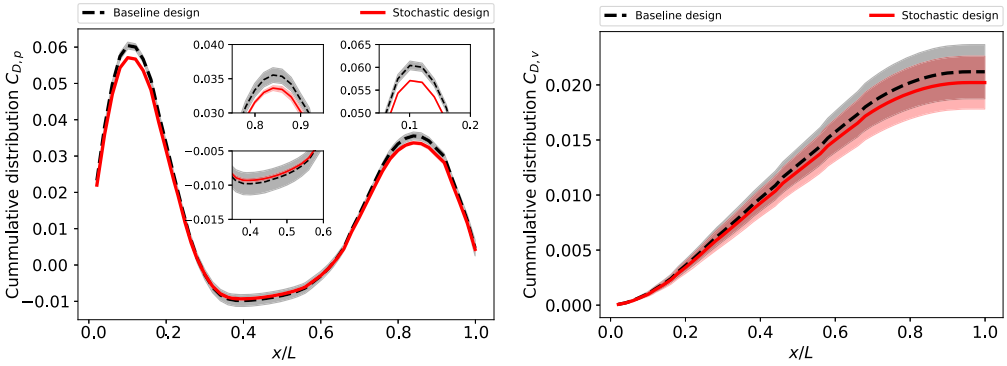

(a) Pressure contributions (b) Viscous contributions

Fig. 7. Drag coefficient cumulative distribution along the airship length. The lines are the mean value, and the shading represents the confidence interval.

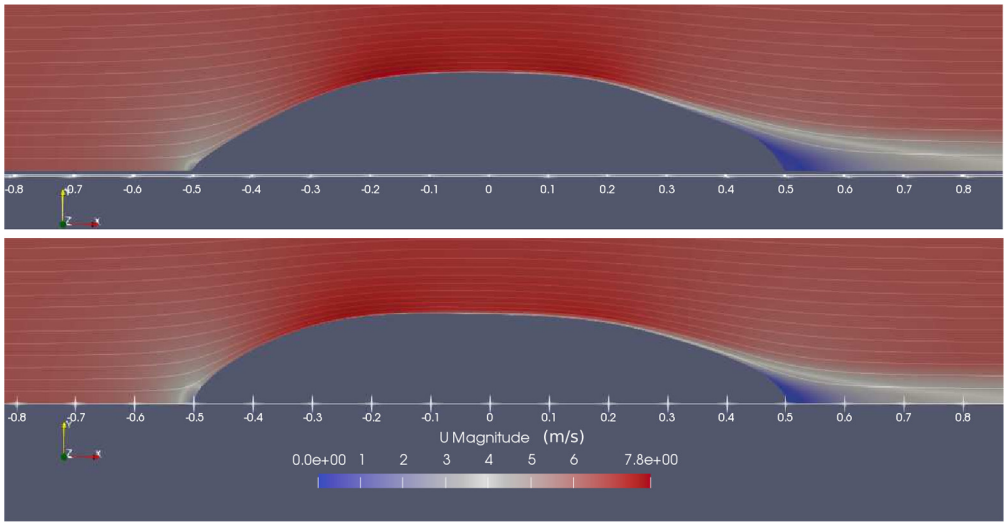

Fig. 8. Velocity field for the optimal design (top) and baseline design (bottom). (For interpretation of the colors in the figure(s), the reader is referred to the web version of this article.)

ter to choose a method that could find global minima. Thus, the solver selected was the differential evolution algorithm described by Storn & Price [53] and implemented in Scipy [54].

The optimal geometry is shown in Fig. 5. The thickness ratio (defined as the maximum diameter divided by the total length) of the optimal design is 8% greater than in the baseline design (0.165 vs. 0.152). Furthermore, the localization of the maximum thickness moves rearwards: in the optimal design it is located at $x/L = 0.47$ while in the baseline design it is at $x/L = 0.38$.

Finally, we can verify that the optimal design is actually more robust than the baseline design. In order to check that, a Monte Carlo experiment is performed. For both, the baseline and the optimal design, 10^3 combinations of U and Tu_∞ are generated and evaluated. The $C_{D,v}$ distribution for both designs can be found in Fig. 6. Indeed, the optimal design achieves a mean $C_{D,v}$ of 2.45×10^{-2} instead of the 2.6×10^{-2} achieved by the baseline design, which represents an improvement of the 6%. These values can be computed integrating the PDF, following the Equation:

$$\mu(C_{D,v}) = \int C_{D,v} \varrho_{C_{D,v}} \mathrm{d}C_{D,v} \tag{43}$$

where $\varrho_{C_{V,d}}$ is the PDF of $C_{V,d}$. As the hull contribution to the total drag is between 60-70%, that is equivalent to a 4% reduction of the total drag. Additional improvements can be achieved by optimizing other components such as fins or propellers.

As the optimal design is less flat-nosed than the original one, it is of particular interest to analyze how this affects the viscous and pressure forces that contributes to the drag. Fig. 7 shows the drag coefficient cumulative distribution along the airship length. It proofs how the improvement in $C_{D,v}$ is achieved mainly by the reduction of the viscous drag coefficient.

Fig. 8 shows the velocity field around both airship. The results are in accordance with what was shown in Fig. 7: optimal design achieves reduced overpressure generated at the leading edge in exchange for a slightly increased size of the turbulent wake.

7. Conclusions

This study has presented a methodology to optimize stratospheric airship hulls in an uncertain design scenario. The NIPC theory has been used to compute the mean volumetric drag coefficient of the proposed hull shapes and two sources of uncertainty have been considered: the wind intensity and the turbulence level at the stratosphere. The NIPC theory can be used to evaluate different design geometries and build a kriging metamodel which, finally, can be used to found the optimal design.

As a particular application, the hull geometry of a HAPS airship has been optimized. Operating at 20 km and 30°N, we have used as starting point the geometry of the ZHIYUAN airship for a fixed length of $L = 250$ m and a volume of 7.5×10^5 m^3. That volume is enough to carry about 250 kg of payload. The envelope shape has been discretized using the CST method and the non linear opti-

mization problem was solved using a genetic algorithm. When the uncertainties are considered, the shape is more tail-nose.

Considering that to evaluate every design under the different flight conditions it is required to perform several CFD simulations, an adequate parallelization of the algorithm is desirable, so it can easily escalate for larger cases of study. In this example, each of the quadrature points is simultaneously evaluated in a different computing node, obtaining a relevant reduction in the computational time.

In order to check the utility of the present design method, a Monte Carlo experiment has been done generating numerous samples of wind intensity and turbulence levels. For each sample, the performances of the stochastic and deterministic designs have been computed. The results show that the stochastic design reduces the mission-averaged drag coefficient of the hull by a 6% (approximately, 4% of the total airship drag). This gain is of utmost importance for HAPS operations [10,15].

In total, more than 15000 CFD simulations have been done to perform this study. While that fact might be limiting for many applications, this work is an example of the new possibilities that the increase in computation power is bringing.

Future work will investigate the hull design under more complex operational scenarios, including the effect of more variables such as the surface roughness and how new parallelization schemes can reduce the total computational cost.

Declaration of competing interest

The authors declare that they have no known competing financial interests or personal relationships that could have appeared to influence the work reported in this paper.

Acknowledgements

The authors thankfully acknowledge the computer resources at Castilla y León Supercomputing Center (SCAYLE) and the valuable suggestions of the anonymous referees that helped to enhance the manuscript.

References

[1] J. Gonzalo, D. López, D. Domínguez, A. García, A. Escapa, On the capabilities and limitations of high altitude pseudo-satellites, Prog. Aerosp. Sci. 98 (2018) 37–56.
[2] B. Kirsch, O. Montagnier, Towards the advent of high-altitude pseudo-satellites (haps), in: Disruptive Technology and Defence Innovation Ecosystems, vol. 5, 2019, pp. 181–201.
[3] D. Ma, G. Li, M. Yang, S. Wang, L. Zhang, Shape optimization and experimental research of near space airship, Proc. Inst. Mech. Eng., Part G, J. Aerosp. Eng. 233 (10) (2019) 3589–3602.
[4] G. Li, J. Wang, Shape optimization of near-space airships considering the effect of the propeller, J. Aerosp. Eng. 33 (5) (2020) 04020054.
[5] X.-Y. Sun, T.-E. Li, G.-C. Lin, Y. Wu, A study on the aerodynamic characteristics of a stratospheric airship in its entire flight envelope, Proc. Inst. Mech. Eng., Part G, J. Aerosp. Eng. 232 (5) (2018) 902–921, https://doi.org/10.1177/0954410017723358.
[6] J. Gonzalo, D. Domínguez, A. García-Gutiérrez, A. Escapa, On the development of a parametric aerodynamic model of a stratospheric airship, Aerosp. Sci. Technol. 107 (2020) 106316, https://doi.org/10.1016/j.ast.2020.106316.
[7] P. Gupta, M. Tripathi, R.S. Pant, Aerodynamic analysis of axi-symmetric lighter-than-air vehicles, in: AIAA Aviation 2021 Forum, 2021, p. 2987.
[8] L. Zhang, W. Zhu, H. Du, M. Lv, Multidisciplinary design of high altitude airship based on solar energy optimization, Aerosp. Sci. Technol. 110 (2021) 106440.
[9] L. Zhang, M. Lv, W. Zhu, H. Du, J. Meng, J. Li, Mission-based multidisciplinary optimization of solar-powered hybrid airship, Energy Convers. Manag. 185 (2019) 44–54.
[10] M.I. Alam, R.S. Pant, Multi-objective multidisciplinary design analyses and optimization of high altitude airships, Aerosp. Sci. Technol. 78 (2018) 248–259, https://doi.org/10.1016/j.ast.2018.04.028.
[11] M. Manikandan, R.S. Pant, Conceptual design optimization of high-altitude airship having a tri-lobed envelope, in: R.R. Salagame, P. Ramu, I. Narayanaswamy, D.K. Saxena (Eds.), Advances in Multidisciplinary Analysis and Optimization, Springer Singapore, Singapore, 2020, pp. 49–61.
[12] J.A. Roney, Statistical wind analysis for near-space applications, J. Atmos. Sol.-Terr. Phys. 69 (13) (2007) 1485–1501.
[13] M. Lynch, B. Mandadzhiev, A. Wissa, Bioinspired wingtip devices: a pathway to improve aerodynamic performance during low Reynolds number flight, Bioinspir. Biomim. 13 (3) (2018) 036003, https://doi.org/10.1088/1748-3190/aaac53.
[14] D. Kumar, M. Raisee, C. Lacor, Combination of Polynomial Chaos with Adjoint Formulations for Optimization Under Uncertainties, Springer International Publishing, Cham, 2019, pp. 567–582.
[15] T.D. Economon, F. Palacios, S.R. Copeland, T.W. Lukaczyk, J.J. Alonso, Su2: an open-source suite for multiphysics simulation and design, AIAA J. 54 (3) (2016) 828–846, https://doi.org/10.2514/1.J053813.
[16] A.G. Liatsikouras, V.G. Asouti, K.C. Giannakoglou, G. Pierrot, M. Megahed, Aerodynamic shape optimization under flow uncertainties using non-intrusive polynomial chaos and evolutionary algorithms, in: 2nd ECCOMAS Thematic Conference on Uncertainty Quantification in Computational Sciences and Engineering (UNCECOMP 2017), Rhodes Island, Greece, 2017.
[17] A. Serani, F. Stern, E.F. Campana, M. Diez, Hull-form stochastic optimization via computational-cost reduction methods, Eng. Comput. (2021) 1–25.
[18] Z. Liu, M. Yang, J. Cheng, D. Wu, J. Tan, Meta-model based stochastic isogeometric analysis of composite plates, Int. J. Mech. Sci. 194 (2021) 106194.
[19] D. López, D. Domínguez, J. Gonzalo, Impact of turbulence modelling on external supersonic flow field simulations in rocket aerodynamics, Int. J. Comput. Fluid Dyn. 27 (8–10) (2013) 332–341, https://doi.org/10.1080/10618562.2013.867951.
[20] S. Volpi, M. Diez, N.J. Gaul, H. Song, U. Iemma, K. Choi, E.F. Campana, F. Stern, Development and validation of a dynamic metamodel based on stochastic radial basis functions and uncertainty quantification, Struct. Multidiscip. Optim. 51 (2) (2015) 347–368.
[21] M. Shirzadi, P.A. Mirzaei, M. Naghashzadegan, Improvement of k-epsilon turbulence model for cfd simulation of atmospheric boundary layer around a high-rise building using stochastic optimization and Monte Carlo sampling technique, J. Wind Eng. Ind. Aerodyn. 171 (2017) 366–379.
[22] X. Du, W. Chen, A most probable point-based method for efficient uncertainty analysis, J. Design Manuf. Autom. 4 (1) (2001) 47–66.
[23] C. Piazzola, L. Tamellini, R. Pellegrini, R. Broglia, A. Serani, M. Diez, Comparing multi-index stochastic collocation and multi-fidelity stochastic radial basis functions for forward uncertainty quantification of ship resistance, arXiv preprint, arXiv:2106.00591, 2021.
[24] D. Quagliarella, A. Serani, M. Diez, M. Pisaroni, P. Leyland, L. Montagliani, U. Iemma, N.J. Gaul, J. Shin, D. Wunsch, et al., Benchmarking uncertainty quantification methods using the naca 2412 airfoil with geometrical and operational uncertainties, in: AIAA Aviation 2019 Forum, 2019, p. 3555.
[25] M. Dodson, G.T. Parks, Robust aerodynamic design optimization using polynomial chaos, J. Aircr. 46 (2) (2009) 635–646, https://doi.org/10.2514/1.39419.
[26] A. García-Gutiérrez, J. Gonzalo, D. López, A. Delgado, Stochastic design of high altitude propellers, Aerosp. Sci. Technol. 107 (2020) 106283, https://doi.org/10.1016/j.ast.2020.106283.
[27] S. Hijazi, G. Stabile, A. Mola, G. Rozza, Non-intrusive polynomial chaos method applied to full-order and reduced problems in computational fluid dynamics: a comparison and perspectives, in: Quantification of Uncertainty: Improving Efficiency and Technology, Springer, 2020, pp. 217–240.
[28] X. Du, L. Leifsson, Optimum aerodynamic shape design under uncertainty by utility theory and metamodeling, Aerosp. Sci. Technol. 95 (2019) 105464.
[29] C.A. Mader, J.R.R.A. Martins, Stability-constrained aerodynamic shape optimization of flying wings, J. Aircr. 50 (5) (2013) 1431–1449, https://doi.org/10.2514/1.C031956.
[30] B. Kulfan, J. Bussoletti, “Fundamental” parametric geometry representations for aircraft component shapes, https://doi.org/10.2514/6.2006-6948, 2006, pp. 1–10.
[31] B. Kulfan, Recent extensions and applications of the “CST” universal parametric geometry representation method, in: 7th AIAA Aviation Technology, Integration and Operations Conference, 2012, pp. 1–10, Ch. 5.
[32] D.R. Jones, A taxonomy of global optimization methods based on response surfaces, J. Glob. Optim. 21 (4) (2001) 345–383.
[33] A. Forrester, A. Sobester, A. Keane, Engineering Design via Surrogate Modelling: A Practical Guide, John Wiley & Sons, 2008.
[34] L. Yaohui, A kriging-based global optimization method using multi-points infill search criterion, J. Algorithms Comput. Technol. 11 (2017) 174830181772530, https://doi.org/10.1177/1748301817725307.
[35] J. Liu, Z.-H. Han, W. Song, Comparison of infill sampling criteria in kriging-based aerodynamic optimization, in: 28th Congress of the International Council of the Aeronautical Sciences 2012, ICAS 2012 2, 2012, pp. 1625–1634.
[36] C. Paulson, G. Ragkousis, Pykriging: a python kriging toolkit, https://doi.org/10.5281/zenodo.21389, Jul. 2015.
[37] H. Chen, L. He, W. Qian, S. Wang, Multiple aerodynamic coefficient prediction of airfoils using a convolutional neural network, Symmetry 12 (4) (2020), https://doi.org/10.3390/sym12040544.

[38] A.L. Habermann, R. Zahn, A. Seitz, M. Hornung, Multidimensional parametric study of a propulsive fuselage concept using OpenFOAM, https://doi.org/10.2514/6.2020-2754.
[39] M.D. Reddy, R.S. Pant, CFD analysis of axisymmetric bodies of revolution using OpenFOAM, https://doi.org/10.2514/6.2018-3334.
[40] C. Suvanjumrat, Comparison of turbulence models for flow past naca0015 airfoil using openfoam, Eng. J. 21 (3) (2017) 207–221.
[41] G. Joubert, J.-F. Roy, Open-source cfd code assessment for lighter-than-air aerodynamic flows simulations, 2017.
[42] G. Chen, Q. Xiong, P.J. Morris, E.G. Paterson, A. Sergeev, Y. Wang, Openfoam for computational fluid dynamics, Not. Am. Math. Soc. 61 (4) (2014) 354–363.
[43] G. Carbone, G. Martinat, D. Farcy, J.-L. Harion, Aerodynamic investigation of a 3.5:1 prolate spheroid, in: AIAA Aviation 2020 Forum, 2020, p. 3053.
[44] Cui Yanxiang, Yang Yanchu, Zhou Jianghua, Zhang Xiangqiang, Yan feng, Numerical aerodynamic investigations on stratospheric airships of different tail configurations, in: 2015 IEEE Aerospace Conference, 2015, pp. 1–9.
[45] F.R. Menter, Improved two-equation k-omega turbulence models for aerodynamic flows, NASA STI/Recon Technical Report N 93, 1992, p. 22809.
[46] Y.K. Chen, X. Zhang, Cfd-rans model validation of turbulent flow: a case study on maat airship, in: Proceedings of 2014 International Conference on Modelling, Identification Control, 2014, pp. 254–258.
[47] F.R. Menter, Two-equation eddy-viscosity turbulence models for engineering applications, AIAA J. 32 (8) (1994) 1598–1605.
[48] X.-L. Wang, G.-Y. Fu, D.-P. Duan, X.-X. Shan, Experimental investigations on aerodynamic characteristics of the zhiyuan-1 airship, J. Aircr. 47 (4) (2010) 1463–1468.
[49] R.L. Iman, Latin Hypercube Sampling, Wiley StatsRef: Statistics Reference Online, 2014.
[50] A. García-Gutiérrez, J. Gonzalo, D. Domínguez, D. López, A. Escapa, Aerodynamic optimization of propellers for high altitude pseudo-satellites, Aerosp. Sci. Technol. 96 (2020) 105562, https://doi.org/10.1016/j.ast.2019.105562.
[51] E. Kalnay, M. Kanamitsu, R. Kistler, W. Collins, D. Deaven, L. Gandin, M. Iredell, S. Saha, G. White, J. Woollen, et al., The ncep/ncar 40-year reanalysis project, Bull. Am. Meteorol. Soc. 77 (3) (1996) 437–472.
[52] J. Sacks, W.J. Welch, T.J. Mitchell, H.P. Wynn, Design and analysis of computer experiments, Stat. Sci. (1989) 409–423.
[53] R. Storn, K. Price, Differential evolution–a simple and efficient heuristic for global optimization over continuous spaces, J. Glob. Optim. 11 (4) (1997) 341–359.
[54] P. Virtanen, R. Gommers, E. Burovski, T.E. Oliphant, D. Cournapeau, W. Weckesser, P. Peterson, N. Mayorov, S. van der Walt, J. Wilson, et al., scipy/scipy: Scipy 1.2.1, Zenodo, 2019.